8328 *Macromolecules* **2009**, *42*, 8328–8334
DOI: 10.1021/ma901612w

Macromolecules
ARTICLE

Carbon Nanotubes−Polypropylene Nanocomposites for Electrostatic Discharge Applications

Jong-Il Lee, Seung-Bo Yang, and Hee-Tae Jung*

National Research Laboratory for Organic Optoelectronic Materials, Department of Chemical & Biomolecular Engineering (BK-21), Korea Advanced Institute of Science and Technology, 373-1 Guseong-dong, Yuseong-gu, Daejeon 305-701, Republic of Korea

Received July 22, 2009; Revised Manuscript Received October 5, 2009

ABSTRACT: We report a novel method for enhancing the dispersion of modified multiwalled carbon nanotubes (MWNTs) in a polypropylene (PP) matrix for electrostatic discharge applications. The surfaces of MWNTs were modified with octadecylamine (ODA) via CF_4 plasma-assisted fluorination and subsequent alkylamination. The number of fluorine groups on the MWNT surface was controlled by varying the CF_4 plasma treatment conditions. Fourier transform infrared spectroscopy (FT-IR) and X-ray photoelectron spectroscopy (XPS) revealed that reaction of the fluorinated MWNTs and octadecylamine (ODA) was strongly affected by solvent quality and reaction temperature. The resulting MWNT/PP nanocomposites exhibited a much finer dispersion in the insulating PP matrix than was observed for nonmodified MWNTs, leading to an enhanced electrical conductance at low MWNT loading (2 wt %). Furthermore, the nanocomposites showed significantly improved mechanical properties; the storage modulus (G') and complex viscosity (η^*) increased significantly in the low-frequency region as MWNT loading was increased, showing a rheological percolation threshold at 1 wt % MWNT loading. This effective method can be applied to the fabrication of other carbon nanotube-based polymer nanocomposites for potential development into electrostatic dissipative (ESD) materials with high mechanical strength and for other high-performance industrial applications.

Introduction

Carbon nanotube (CNT)-based polymer nanocomposites constitute one of the successful applications of CNTs developed in the CNT research community. Because of their extraordinary electrical, mechanical, and thermal properties, CNTs enable the development of multifunctional composites by incorporating nanotubes into a variety of polymer matrices.[1−5] Achieving a uniform dispersion of the nanotubes in the polymer matrix can enhance the electrical and mechanical properties at low nanotube loadings compared to other conventional additives, such as carbon black and carbon fiber, primarily due to the high aspect ratio of the nanotubes.[6−9] It has been reported that the electrical,[10,14] mechanical,[15,16] rheological,[39,41] and thermal[11−13] properties improved considerably when modified nanotubes were finely dispersed in the polymer matrix. For example, the electrical properties of polycarbonate (PC) were enhanced by dispersing single-walled carbon nanotubes (SWNTs) into the polymer matrix.[14] Nanocomposites of polyethylene fibers and modified SWNTs exhibited excellent mechanical properties, with a tensile modulus of 1.25 GPa after addition of a small quantity of SWNTs (5 wt %).[15] A superior tensile modulus and yield strength of poly(ethylene oxide) were also obtained by incorporating CNTs into the polymer.[16]

For such applications, it is essential to obtain a fine dispersion of nanotubes using polymer binders. Various approaches have been developed for enhancing dispersion, including covalent sidewall functionalization of CNTs,[17−20] noncovalent sidewall functionalization of CNTs,[21,22] in situ polymerization of monomers with nanotubes,[23,24] polymer wrapping,[25] and solution blending.[26−28] Among these methods, the introduction of hydrophobic organic molecules with long alkyl chains onto nanotube surfaces is reported to be one of the most effective ways of achieving highly efficient interfacial interactions between nanotubes and hydrophobic polymers such as polyolefins, including polypropylene and polyethylene. In order to attach the alkyl chains to nanotubes, several methods, including a 1,3-dipolar cycloaddition reaction that forms pyrrolidine-fused rings,[17,29] acid treatment followed by reaction with aliphatic amines[30] (or aliphatic bromide[31]), and an addition reaction of undecyl radicals generated by thermal decomposition of lauroyl peroxide,[32] have been suggested for the preparing alkyl-modified nanotubes.

Here, we report on a novel method for achieving a highly efficient fine dispersion of modified MWNTs in a polymeric matrix for potential application to electrostatic discharge (ESD) and electromagnetic interference (EMI) shielding materials. The surfaces of MWNTs were modified by alkylamination of fluorinated MWNTs in the presence of octadecylamine (ODA) under sonication to generate octadecylamino ($C_{18}H_{37}N$) chains on the nanotube surfaces. The fluorinated MWNT surfaces were prepared by CF_4 plasma treatment. We used polypropylene (PP) as a polymeric matrix because it is one of the most versatile thermoplastic polymers used in a wide range of applications: packaging, automotive parts, electrical home appliances, and low-cost industrial parts. We demonstrate that the octadecylamino-functionalized MWNTs were finely dispersed in PP, resulting in a significant improvement of electrical and rheological properties at low nanotube content (~2 wt %). This method provides a route for fabricating CNT/polymer nanocomposites that is much simpler than previous alkylation methods such as acid treatment.[30,31]

Experimental Section

Materials. Commercially available multiwalled nanotubes (Baytubes C150 HP, Bayer Material Science, 99% purity, length: 1−10 μm, outer mean diameter: 13−16 nm), synthesized

*To whom correspondence should be addressed: Tel +82-42-350-3931, Fax +82-42-350-3910, e-mail heetae@kaist.ac.kr.

 Published on Web 10/13/2009

Scheme 1. Experimental Scheme for Preparation of (a) ODA-MWNT and (b) MWNT/PP Nanocomposites

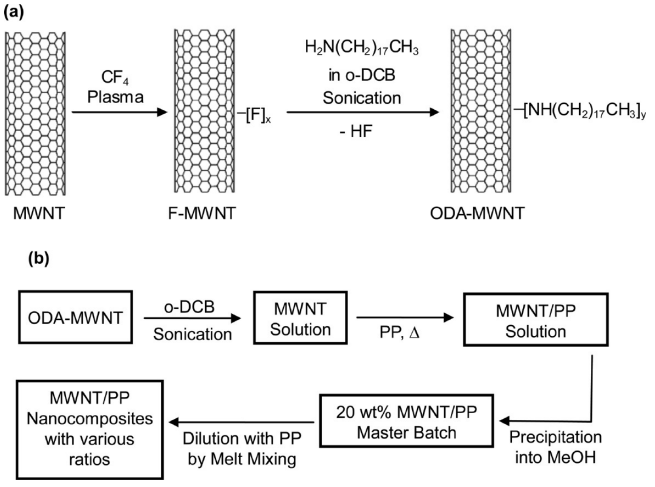

by catalytic chemical vapor deposition, were used in this study. A polypropylene copolymer (Kopelen JM-370, Honam Petrochemical Corp., melt-flow index (MFI) 31.4 g/10 min at 230 °C and 2.16 kg load, 7.5 wt % ethylene content) was used for the matrix polymer. Polypropylene copolymer contains small quantities of heterophasic structures of poly(ethylene-*co*-propylene) rubber (EPR) that improve impact strength at low temperatures[33] and enable conventional polypropylene to withstand high impacts. A commercially available octadecylamine (ODA, $CH_3(CH_2)_{17}NH_2$, Sigma-Aldrich Chemicals, 97%) was used as received.

Preparation of ODA-Modified MWNTs. The preparation route for the fluorinated MWNTs (F-MWNTs) and ODA-modified MWNTs (ODA-MWNTs) is described in Scheme 1a. In order to modify ODA molecules on the MWNT surface, the surfaces of MWNTs were first fluorinated by plasma-assisted decomposition of CF_4[34,35] with a 13.56 MHz radio-frequency plasma source (VSRIE-600A, Vacuum Sciences). This method is very efficient for modifying CNT surfaces with fluorinated groups because such surface treatments do not damage the CNTs as significantly as other conventional fluorination methods, such as application of elemental fluorine at high temperatures.[36] The plasma treatment was carried out at room temperature with CF_4 gas pressures of 5×10^{-2} Torr. The CF_4 flow rate was held constant at 60 sccm with various plasma powers and times. The F-MWNTs were dispersed into 1,2-dichlorobenzene (o-DCB) by sonication (42 kHz, 135 W) for 1 h at room temperature. Then, ODA (20 g) and pyridine (Py, 3 mL, as a catalyst) were added to the dispersed F-MWNT solution. The resulting mixture was reacted under sonication in a nitrogen atmosphere for 5 h at a range of temperatures, from room temperature to 60 °C. After completion of the alkylamination reaction, the solution was filtered on a 0.2 μm pore size Teflon membrane (Advantec); the resulting ODA-MWNTs were washed with large amounts of chloroform to remove residual ODA and dried overnight in a vacuum oven at 120 °C.

Preparation of MWNT/PP Nanocomposites. The ODA-MWNTs were dispersed in o-DCB by sonication at room temperature for 1 h. PP was added to the dispersed MWNT solution at 190 °C under a nitrogen atmosphere and vigorously stirred for 1 h. The solution was precipitated in a large volume of methanol. The precipitate was isolated by filtration and washed several times with methanol to remove residual o-DCB. The resulting powder sample, with a MWNT concentration of 20 wt %, was placed in a vacuum oven at 80 °C for 12 h. The MWNT concentration of the MWNT/PP nanocomposites was varied by adding PP to the prepared 20 wt % composite via melt blending, in which melt mixing was performed with an internal mixer (Brabender PLASTI-CORDER PL-2200) at 190 °C, 100 rpm for 10 min. Nanocomposite products of eight concentrations were prepared by these procedures (illustrated in Scheme 1b).

Characterization. Fourier transform infrared spectroscopy (FT-IR), X-ray photoelectron spectroscopy (XPS), and Raman spectroscopy were used to identify the chemical structure of the modified MWNTs. FT-IR examined absorption bands between 1000 and 4000 cm^{-1} on a Magna 550 FT-IR spectrometer (Nicolet). XPS was carried out on ESCA 2000 XPS (Thermo VG Scientific) using a monochromatic (Mg Kα = 1253.6 eV) source. Raman spectroscopy was carried out on an FT-Raman spectrometer (Bruker) with 1064 nm laser illumination to investigate the structural changes of nanotubes. Thermogravimetric analysis (TGA) was performed on TGA 2950 (TA Instruments) in a nitrogen atmosphere at 20 °C/min heating rate. Specimens for transmission electron microscopy (TEM, Tecnai F20, Philips) imaging were prepared by ultramicrotoming at room temperature. Polarized optical microscopy (POM) images of the nanocomposites were taken on an optical microscope with a cross-polarizer (DM LB, Leica). Surface resistivity was measured by an ultrahigh-resistance meter (R8340, Advantest). Rheological behavior was measured by an advanced rheometric expansion system (ARES, TA Instruments) in oscillatory shear at 10% strain in the parallel-plate geometry with a 25 mm plate under a dry nitrogen atmosphere. Specimens for rheological measurements were prepared with a 2 mm thick disk. Frequency sweeps from 0.01 to 500 rad/s were carried out at 230 °C in consideration of the test temperature of MFI for PP which is measured at 230 °C according to ASTM D-1238 providing simple rheological properties generally used in the field of PP industry.

Results and Discussion

Figure 1a shows FT-IR spectra of F-MWNT that were generated by CF_4 plasma treatment on the MWNTs. The sharp peak at 1545 cm^{-1} was assigned to the stretching mode of the C=C double bond that arose from the framework of the nanotube sidewalls. After plasma treatment, a new peak appeared at 1221 cm^{-1}, corresponding to a C−F stretch mode, confirming the generation of F-MWNTs.[34]

We found that CF_4 plasma treatment conditions strongly affected the surface fluorination of MWNTs. Figure 1b,c shows the normalized XPS spectra of F-MWNTs as functions of plasma powers and times. The spectrum of the fluorinated MWNTs contained a maximum at 684.9 eV that is attributed to the covalent attachment of fluorine to the MWNT surfaces. To estimate the degree of fluorination of MWNTs under various plasma treatment conditions, the molar ratios of fluorine and carbon atoms (F/C) were determined by measuring relative peak areas of F 1s (684.9 eV) and C 1s (284.5 eV) bands on the basis of the linear background intensity and atomic sensitivity factor.[37] When the plasma exposure time was increased from 30 to 50 min at a power of 50 W, the F/C ratio increased from 0.04 to 0.06, indicating enhanced fluorination on MWNTs. Also, the F/C ratio increased from 0.06 to 0.10 as the plasma treatment power was increased from 50 to 100 W at an exposure time of 50 min. Thus, relatively high power and long exposure times for plasma treatment generated large amounts of fluorine on MWNT surfaces. However, the XPS spectra of carbon in Figure 1b do not show a significant C−F signal at 288.4 eV. In general, it is required that F/C ratio is above 0.3 to show noticeable C−F bond signal on XPS of carbon.[35] Therefore, the very weak C−F bond signal at 288.4 eV is due to relatively low fluorine content on the MWNT, since the F/C ratios of the F-MWNT are in the range of 0.04−0.10 (Figure 1c).

Raman spectra were used to investigate structural changes after CF_4 plasma exposure with different plasma powers and

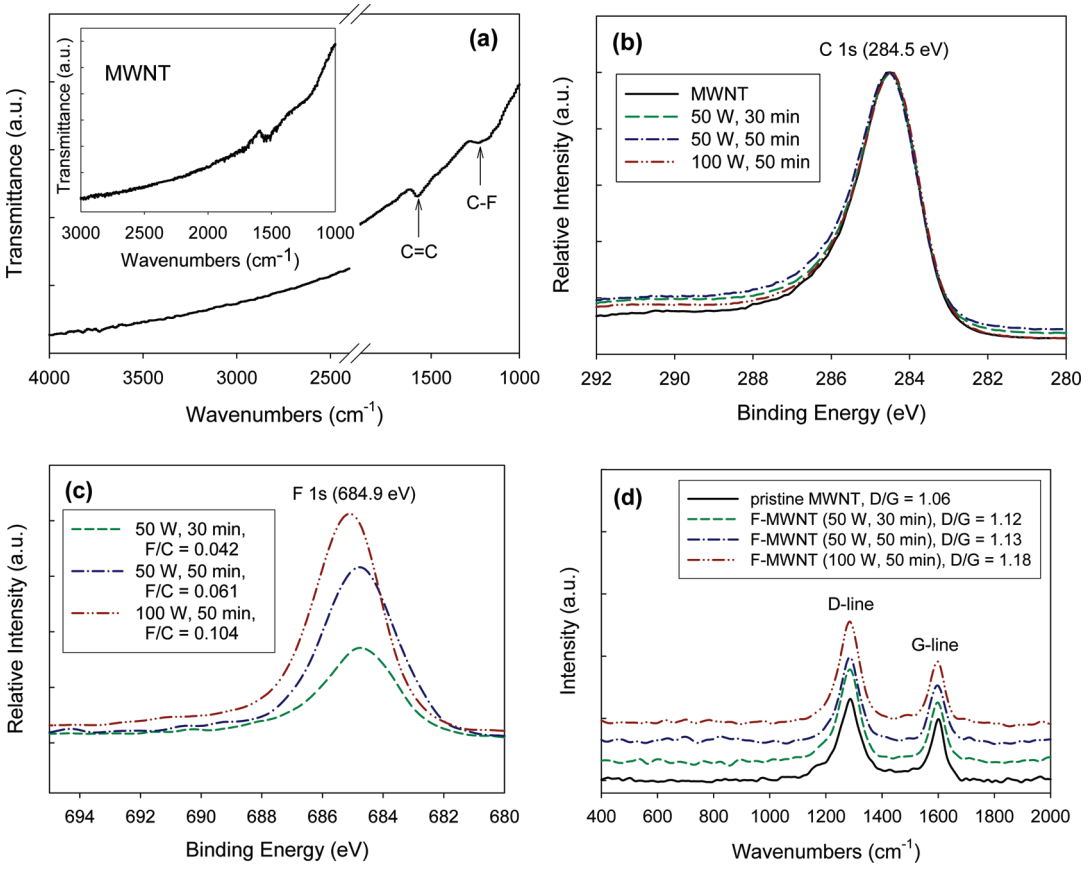

Figure 1. Characteristics of F-MWNT. (a) FT-IR spectra of F-MWNT under the plasma condition of 50 W, 50 min (the inset shows the FT-IR spectrum of pristine MWNT). XPS spectra of (b) C 1s (284.5 eV) and (c) F 1s (684.9 eV) for F-MWNT with variation of plasma treatment power and time. (d) Raman spectra of pristine MWNT and F-MWNT with variation of plasma treatment power and time.

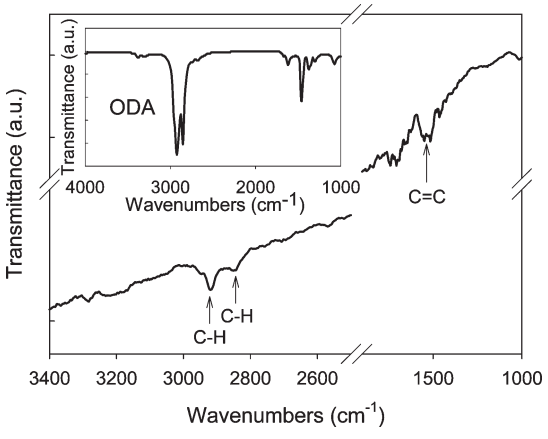

Figure 2. FT-IR spectra of ODA-MWNT (the inset shows the FT-IR spectrum of ODA).

times (Figure 1d). The G-line at 1600 cm^{-1}, corresponding to sp^2 bonding, and the D-line at 1280 cm^{-1}, corresponding to sp^3 bonding, are evident in the spectra. The relative intensity ratios of the D/G bands, which represent the degree of disorder in F-MWNT, did not change much after CF_4 plasma treatment. Thus, it is likely that the fluorination primarily occurred at defect sites in pristine MWNTs. Thus, the degree of fluorination was strongly affected by plasma power and time, and plasma treatment did not increase the number of defect sites on MWNTs.

The ODA-modified MWNTs were obtained by alkylamination of F-MWNTs and ODA molecules. Figure 2 shows FT-IR spectra of ODA-MWNTs in o-DCB at 60 °C. The absorption band at 1221 cm^{-1}, which is ascribed to the C−F bond, disappeared after the alkylamination reaction with ODA. Moreover, new peaks appeared in the range of 3000−2800 cm^{-1} due to a C−H stretch mode (CH_2 antisymmetric stretch at 2920 cm^{-1}, CH_2 symmetric stretch at 2851 cm^{-1}), providing clear evidence of octadecylamino modification on the MWNT surfaces. It is noteworthy that the surface modification of ODA molecules is strongly influenced by the solvent quality and reaction temperature. XPS spectra of the ODA-MWNTs prepared in a variety of solvents and temperatures (Supporting Information, Figure S1) show that o-DCB at 60 °C is a suitable reaction condition for alkylamination on the MWNT surfaces.

The N−H stretch around 3200−3300 cm^{-1} on the FT-IR spectrum of ODA-MWNT is due to not only primary amine from free ODA but also secondary amine from covalently attached octadecylamino ($C_{18}H_{37}N$) chain.[34] Therefore, TGA curves (Figure 3) were used to provide additional evidence for covalently attachment of octadecylamino molecules on the MWNT surface and determine the degree of alkylamination on the MWNT surfaces. The thermogram of ODA-MWNT shows two-step decomposition at 200−500 and 500−900 °C. The first step of weight loss at 200−500 °C is due to decomposition of alkyl chains on the MWNT surface. However, the thermogram of pure ODA shows steep weight loss due to organics decomposition in the temperature range of 150−250 °C. This result supports the fact that the octadecylamino molecules are covalently attached on the nanotubes. In consideration of weight loss at 200−500 °C by decomposition of alkyl chains, the degree of alkylamination on the MWNT surfaces is determined to be ~8 wt %.

Figure 4 shows the surface resistivity of the composites as a function of MWNT loading. The concentrations of MWNT in

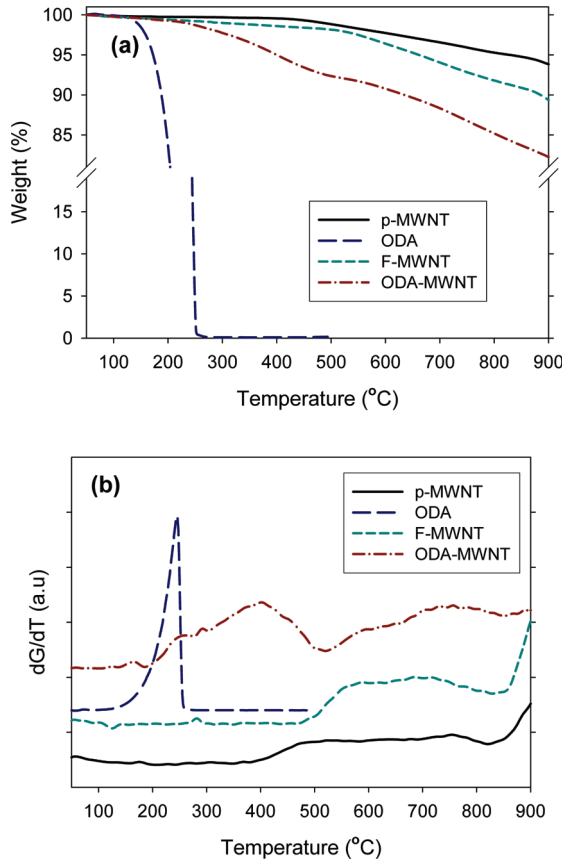

Figure 3. (a) TGA curves and (b) their derivative curves of pristine MWNT, ODA, F-MWNT, and ODA-MWNT.

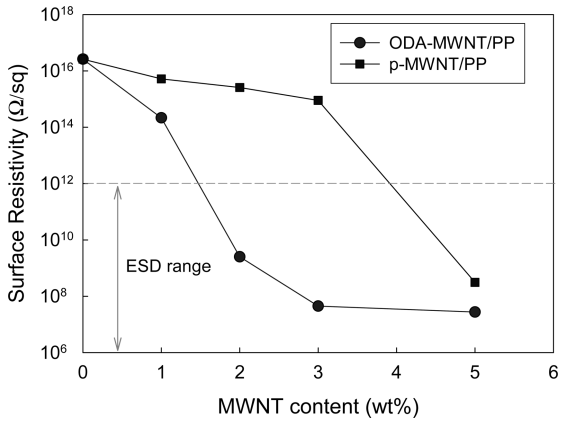

Figure 4. Surface resistivity of MWNT/PP composites filled with ODA-MWNT or p-MWNT as a function of the nanotube loading.

the nanocomposites range from 1 to 5 wt %, prepared by melt blending of neat PP and the 20 wt % MWNT master batch (Supporting Information, Figure S2). The pristine MWNT/PP nanocomposites show that resistivity gradually decreased from 0 to 3 wt % MWNT loading, followed by a dramatic reduction at higher MWNT loadings. In the case of ODA-modified MWNT/PP nanocomposites, however, surface resistivity dramatically decreased at low MWNT loading and leveled out at 3 wt % MWNT loading. However, sharp decreases in surface resistivity were observed for 2 wt % ODA-MWNT composites and 5 wt % p-MWNT composites. This stepwise change in resistivity can be regarded as an electrical percolation threshold. When the nanotube loading reaches a conductivity threshold, a conductive nanotubes network exists in the composite, forming a conductive path. Therefore, the electrical percolation threshold observed for ODA-MWNT/PP nanocomposites was low compared to pristine MWNT/PP, most likely because effective conductive paths are easier to achieve in the fine dispersion of modified MWNT in PP. Thus, a low loading level of 2 wt % ODA-MWNT in ODA-MWNT/PP composites is required for potential applications to ESD because surface resistivity in ESD applications must be in the range of 10^6-10^{12} Ω/sq.[38] In general, low MWNT loading for ESD materials not only leads to amelioration of the sloughing problems that are present in high MWNT loading but also is more economically efficient because the need for expensive fillers such as carbon nanotubes is reduced.

Enhanced electrical properties of the ODA-MWNT/PP nanocomposites result from a dispersion of ODA-MWNTs in PP matrices that is much finer than the dispersion of p-MWNTs. TEM and POM (Figure 5) images clearly show that ODA-MWNTs yield enhanced dispersion in PP matrices compared to pristine MWNTs. TEM images of ODA-MWNTs/PP nanocomposites (1 wt % ODA-MWNTs) (Figure 5a) show that the introduction of long alkyl chains on MWNTs significantly improves the dispersion of MWNTs relative to the p-MWNTs (Figure 5b). A comparison of POM textures of neat PP (Figure 5c), ODA-MWNT/PP (Figure 5d), and p-MWNT/PP (Figure 5e) provides further evidence for this conclusion. Large spherulites were observed in neat PP, with an average diameter of 200 μm. The size of the spherulites was smaller in p-MWNT/PP nanocomposites, with an average diameter of 100 μm. The spherulite size was further reduced to 50 μm in ODA-MWNT/PP (1 wt % ODA-MWNT). Such size reductions were attributed to the fact that the nanotubes act as nucleating sites for crystallization of PP, and thus smaller spherulites of ODA-MWNT/PP arose from a better dispersion of nanotubes.

We measured the rheological properties of the p-MWNT/PP and ODA-MWNT/PP nanocomposites to characterize the percolated network structure, dispersion state of MWNTs, and interaction between fillers and polymer matrix.[39−41] In addition, rheological properties give insights into the mechanical properties and processability. Figure 6 shows the storage modulus (G') and loss modulus (G'') of the p-MWNT/PP composites (Figure 6a,b) and the ODA-MWNT/PP composites (Figure 6c,d). The storage modulus (G') of the p-MWNT/PP composites increased with increasing MWNT content. The ODA-MWNT/PP composites were characterized by a storage modulus at low frequencies that increased more significantly than the p-MWNT/PP composites, suggesting that the rheological properties of MWNT/PP composites were influenced by modification of the MWNT.

The loss modulus (G'') of the p-MWNT/PP composites increased with increasing MWNT content. Also, the loss modulus at low frequencies for the ODA-MWNT/PP composites increased more significantly than for the p-MWNT/PP composites. From the results presented in Figure 6, it can be seen that the storage modulus increase for the MWNT/PP composites was greater than the loss modulus increase for the MWNT/PP composites. This observation can be explained by considering that the structure of polymer composites is reflected more sensitively by the storage modulus (G') than the loss modulus (G'').[42−44]

The complex viscosity (η^*), shown in Figure 7, indicated that neat PP showed typical Newtonian behavior at low frequencies and shear thinning behavior at high shear rates. However, composites containing nanotubes showed higher complex viscosity and earlier shear thinning behavior than neat PP. These effects were markedly increased for ODA-MWNT/PP composites and at higher nanotube loadings due to a uniform dispersion of nanotubes and enhanced interaction between the PP matrix and ODA-MWNTs. The rheological properties of polymer composites reflect a hydrodynamically percolated filler−filler network structure at low frequencies (the terminal region) and

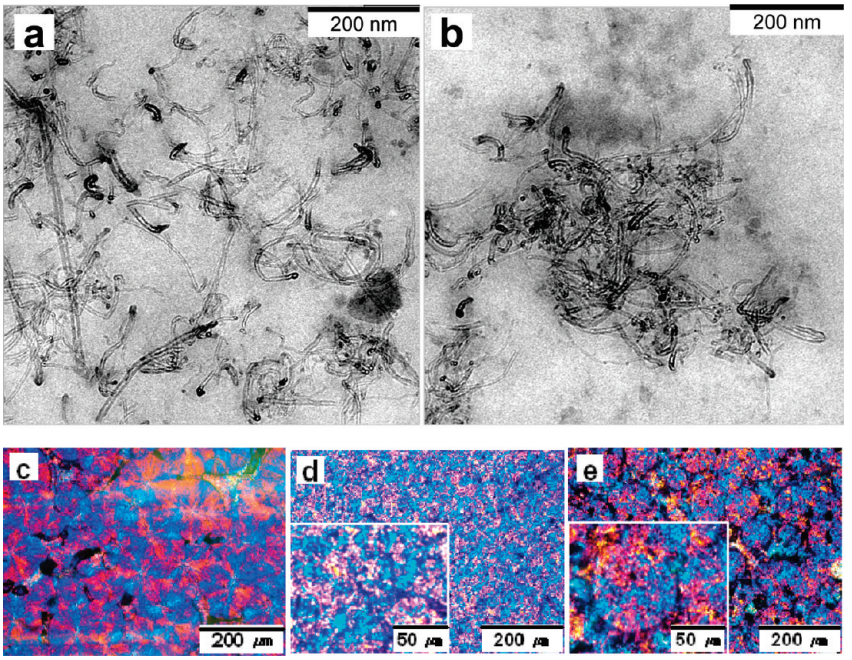

Figure 5. Morphology of the MWNT/PP composites. TEM images of (a) 1 wt % ODA-MWNT/PP composites and (b) 1 wt % p-MWNT/PP composites. POM images of (c) PP, (d) 1 wt % ODA-MWNT/PP composites, and (e) 1 wt % p-MWNT/PP composites.

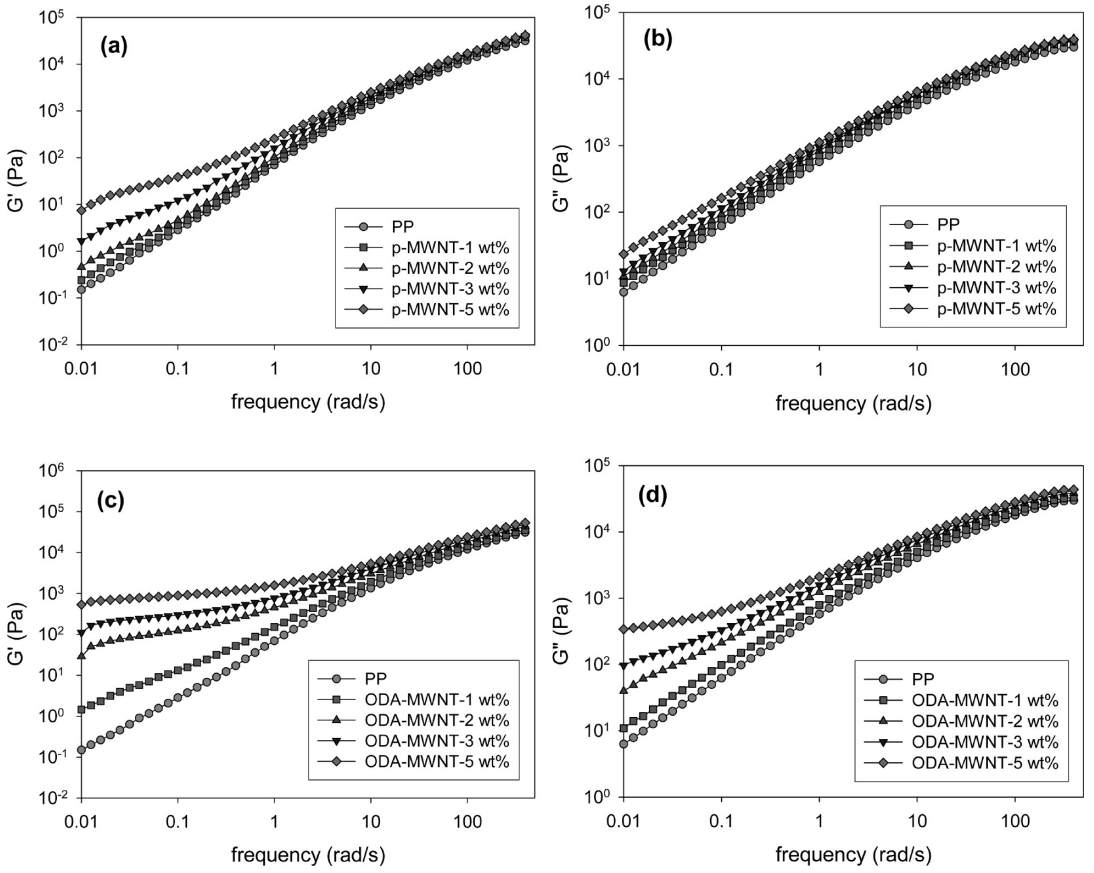

Figure 6. (a) Storage modulus (G') and (b) loss modulus (G'') of p-MWNT/PP composites. (c) Storage modulus (G') and (d) loss modulus (G'') of ODA-MWNT/PP composites.

the dynamics of polymer entanglement at high frequencies.[39−41] Therefore, increases in the rheological properties of nanotube composites at low frequencies were related to increased connections between nanotubes in the nanotube−nanotube network structure formed by linking the random coils of polymer chains, which results in impeded polymer chain motion.

Figure 8 shows the storage modulus at 0.1 rad/s as a function of MWNT content. The rheological percolation of the ODA-MWNT

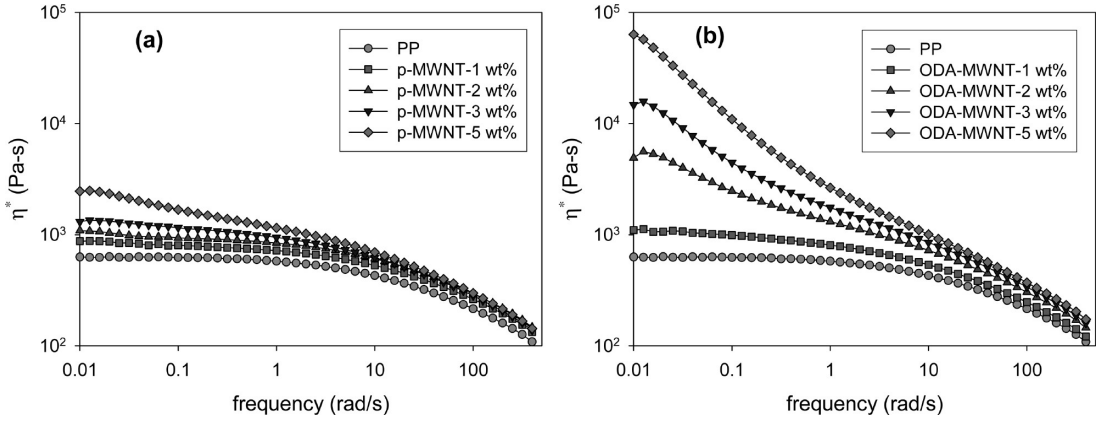

Figure 7. Complex viscosity (η^*) of (a) p-MWNT/PP composites and (b) ODA-MWNT/PP composites.

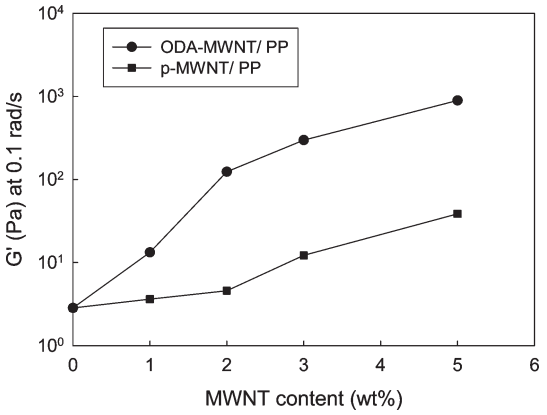

Figure 8. Storage modulus (G') of MWNT/PP composites filled with p-MWNT or ODA-MWNT as a function of the nanotube loading at a fixed frequency of 0.1 rad/s.

composites appeared at 1 wt % nanotube loading, while that of the p-MWNT composites appeared between 2 and 3 wt %. As previously reported,[41,45−48] such different values between electrical percolation and rheological percolation can be attributed to the fact that the nanotube−nanotube distance for electrical conductivity percolation is shorter than for rheological percolation.

Conclusions

We prepared ODA-modified MWNTs, enabling the preparation of a fine dispersion of MWNTs in a PP matrix, by fluorination of the MWNTs using CF_4 plasma treatment and subsequent reaction with ODA under sonication. The electrical and rheological properties of the resulting ODA-MWNT/PP nanocomposites were significantly enhanced, characterized by a percolation threshold of 1−2 wt % nanotube loading, while the percolation threshold of p-MWNT/PP composites was measured to be 3−5 wt %. Microscopic imaging showed that this was due to a finer dispersion of ODA-modified MWNTs. Unlike previous fabrication methods, this approach provides a method for the easy alkylamination of nanotubes with low carbon damage. The ODA-MWNT composites showed lower electrical and rheological percolation thresholds than pristine MWNT/PP composites.

Acknowledgment. This work was supported by the Honam Petrochemical Corporation and the Center for Nanoscale Mechatronics & Manufacturing (08K140100414, CNMM).

Supporting Information Available: XPS spectra of C 1s (284.5 eV) and N 1s (398.1 eV) corresponding to the C−N linkage of ODA-MWNT prepared under different solvent and temperature; TGA curves of ODA-MWNT/PP composites and pristine-MWNT/PP composites. This material is available free of charge via the Internet at http://pubs.acs.org.

References and Notes

(1) Milo, S. P. S.; Alan, H. W. *Adv. Mater.* **1999**, *11*, 937–941.
(2) Baughman, R. H.; Zakhidov, A. A.; de Heer, W. A. *Science* **2002**, *297*, 787–792.
(3) Koerner, H.; Price, G.; Pearce, N. A.; Alexander, M.; Vaia, R. A. *Nat. Mater.* **2004**, *3*, 115–120.
(4) Moniruzzaman, M.; Winey, K. I. *Macromolecules* **2006**, *39*, 5194–5205.
(5) Ajayan, P. M.; Tour, J. M. *Nature* **2007**, *447*, 1066–1068.
(6) Manchado, M. A. L.; Valentini, L.; Biagiotti, J.; Kenny, J. M. *Carbon* **2005**, *43*, 1499–1505.
(7) Coleman, J. N.; Khan, U.; Gun'ko, Y. K. *Adv. Mater.* **2006**, *18*, 689–706.
(8) Paul, D. R.; Robeson, L. M. *Polymer* **2008**, *49*, 3187–3204.
(9) Das, N. C.; Maiti, S. *J. Mater. Sci.* **2008**, *43*, 1920–1925.
(10) Barrau, S.; Demont, P.; Perez, E.; Peigney, A.; Laurent, C.; Lacabanne, C. *Macromolecules* **2003**, *36*, 9678–9680.
(11) Biercuk, M. J.; Llaguno, M. C.; Radosavljevic, M.; Hyun, J. K.; Johnson, A. T.; Fischer, J. E. *Appl. Phys. Lett.* **2002**, *80*, 2767–2769.
(12) Choi, E. S.; Brooks, J. S.; Eaton, D. L.; Al-Haik, M. S.; Hussaini, M. Y.; Garmestani, H.; Li, D.; Dahmen, K. *J. Appl. Phys.* **2003**, *94*, 6034–6039.
(13) Gao, J.; Yu, A.; Itkis, M. E.; Bekyarova, E.; Zhao, B.; Niyogi, S.; Haddon, R. C. *J. Am. Chem. Soc.* **2004**, *126*, 16698–16699.
(14) Ramasubramaniam, R.; Chen, J.; Liu, H. *Appl. Phys. Lett.* **2003**, *83*, 2928–2930.
(15) Haggenmueller, R.; Zhou, W.; Fischer, J. E.; Winey, K. I. *J. Nanosci. Nanotechnol.* **2003**, *3*, 105–110.
(16) Geng, H.; Rosen, R.; Zheng, B.; Shimoda, H.; Fleming, L.; Liu, J.; Zhou, O. *Adv. Mater.* **2002**, *14*, 1387–1390.
(17) Georgakilas, V.; Kordatos, K.; Prato, M.; Guldi, D. M.; Holzinger, M.; Hirsch, A. *J. Am. Chem. Soc.* **2002**, *124*, 760–761.
(18) Dyke, C. A.; Tour, J. M. *J. Phys. Chem. A* **2004**, *108*, 11151–11159.
(19) Blake, R.; Gun'ko, Y. K.; Coleman, J.; Cadek, M.; Fonseca, A.; Nagy, J. B.; Blau, W. J. *J. Am. Chem. Soc.* **2004**, *126*, 10226–10227.
(20) Tasis, D.; Tagmatarchis, N.; Bianco, A.; Prato, M. *Chem. Rev.* **2006**, *106*, 1105–1136.
(21) Chen, R. J.; Zhang, Y.; Wang, D.; Dai, H. *J. Am. Chem. Soc.* **2001**, *123*, 3838–3839.
(22) Chen, J.; Liu, H.; Weimer, W. A.; Halls, M. D.; Waldeck, D. H.; Walker, G. C. *J. Am. Chem. Soc.* **2002**, *124*, 9034–9035.
(23) Bryning, M. B.; Milkie, D. E.; Islam, M. F.; Kikkawa, J. M.; Yodh, A. G. *Appl. Phys. Lett.* **2005**, *87*, 161909/1–161909/3.
(24) Zhu, J.; Kim, J.; Peng, H.; Margrave, J. L.; Khabashesku, V. N.; Barrera, E. V. *Nano Lett.* **2003**, *3*, 1107–1113.
(25) O'Connel, M. J.; Boul, P.; Ericson, L. M.; Huffman, C.; Wang, Y.; Haroz, E.; Kuper, C.; Tour, J.; Ausman, K. D.; Smalley, R. E. *Chem. Phys. Lett.* **2001**, *342*, 265–271.
(26) Sundararajan, P. R.; Singh, S.; Moniruzzaman, M. *Macromolecules* **2004**, *37*, 10208–10211.

(27) Du, F.; Fischer, J. E.; Winey, K. I. *J. Polym. Sci., Part B: Polym. Phys*. **2003**, *41*, 3333–3338.
(28) Singh, S.; Pei, Y.; Miller, R.; Sundararajan, P. R. *Adv. Funct. Mater*. **2003**, *13*, 868–872.
(29) Tagmatarchis, N.; Prato, M. *J. Mater. Chem*. **2004**, *14*, 437–439.
(30) Qin, Y.; Liu, L.; Shi, J.; Wu, W.; Zhang, J.; Guo, Z.-X.; Li, Y.; Zhu, D. *Chem. Mater*. **2003**, *15*, 3256–3260.
(31) Xu, D.; Wang, Z. *Polymer* **2008**, *49*, 330–338.
(32) Koval'chuk, A. A.; Shevchenko, V. G.; Shchegolikhin, A. N.; Nedorezova, P. M.; Klyamkina, A. N.; Aladyshev, A. M. *Macromolecules* **2008**, *41*, 7536–7542.
(33) Del-Duca, D. In *Polypropylene Handbook*, 2nd ed.; Pasquini, N., Ed.; Hanser Publishers: Munich, 2005; pp 314−317.
(34) Valentini, L.; Puglia, D.; Armentano, I.; Kenny, J. M. *Chem. Phys. Lett*. **2005**, *403*, 385–389.
(35) Plank, N. O. V.; Forrest, G. A.; Cheung, R.; Alexander, A. J. *J. Phys. Chem. B* **2005**, *109*, 22096–22101.
(36) Khabashesku, V. N.; Billups, W. E.; Margrave, J. L. *Acc. Chem. Res*. **2002**, *35*, 1087–1095.
(37) Moulder, J. F.; Stickle, W. F.; Sobol, P. E.; Bomben, K. D. In *Handbook of X-ray Photoelectron Spectroscopy*; Chastain, J., Ed.; Perkin-Elmer Corp.: Eden Prairie, MN, 1992; p 25.
(38) Markarian, J. *Plast. Addit. Compd*. **2008**, *10*, 22–25.
(39) Seo, M. K.; Park, S. J. *Chem. Phys. Lett*. **2004**, *395*, 44–48.
(40) Lee, S. H.; Cho, E.; Jeon, S. H.; Youn, J. R. *Carbon* **2007**, *45*, 2810–2822.
(41) Du, F.; Scogna, R. C.; Zhou, W.; Brand, S.; Fischer, J. E.; Winey, K. I. *Macromolecules* **2004**, *37*, 9048–9055.
(42) Pötschke, P.; Fornes, T. D.; Paul, D. R. *Polymer* **2002**, *43*, 3247–3255.
(43) Mitchell, C. A.; Bahr, J. L.; Arepalli, S.; Tour, J. M.; Krishnamoorti, R. *Macromolecules* **2002**, *35*, 8825–8830.
(44) Sung, Y. T.; Han, M. S.; Song, K. H.; Jung, J. W.; Lee, H. S.; Kum, C. K.; Joo, J.; Kim, W. N. *Polymer* **2006**, *47*, 4434–4439.
(45) Hu, G.; Zhao, C.; Zhang, S.; Yang, M.; Wang, Z. *Polymer* **2006**, *47*, 480–488.
(46) Zhang, Q.; Lippits, D. R.; Rastogi, S. *Macromolecules* **2006**, *39*, 658–666.
(47) Hobbie, E. K.; Fry, D. J. *J. Chem. Phys*. **2007**, *126*, 124907.
(48) Zhang, Q.; Rastogi, S.; Chen, D.; Lippits, D.; Lemstra, P. J. *Carbon* **2006**, *44*, 778–785.